

Bio-based semi-aromatic polyamide/functional clay nanocomposites: preparation and properties†

Cite this: *RSC Adv.*, 2014, 4, 23420

Meisam Shabanian,^{bc} Nianjun Kang,^a Jianwen Liu,^b Udo Wagenknecht,^b Gert Heinrich^{bd} and De-Yi Wang^{*a}

In this paper we first describe the design and synthesis of two novel cationic functional modifiers, *i.e.* a functionalized β -cyclodextrin (β -CD) derivative and tris(3-aminophenyl)phenyl phosphine oxide (TAP). Cloisite Na⁺ (clay-Na) and the modifiers were used for the preparation of the organoclay containing phosphine oxide (clay-P=O) and of the organoclay containing β -cyclodextrin (clay-CD) *via* ion-exchange reaction. Biobased semi-aromatic polyamide (BPA)/functional clay (clay-P=O and clay-CD) nanocomposites subsequently were prepared *via* solution blending. Effects of the two different types of organoclays on the flammable, thermal and mechanical properties of these biobased semi-aromatic polyamide nanocomposites were then studied. The properties of the nanocomposites were found to be strongly related to the nature of the modifiers. The clay-CD based nanocomposites (BPACD) showed more enhancements in thermal stability. The modifier containing the phosphine oxide moiety and triamine groups had stronger interactions with the polymer matrix, and exhibited superior mechanical properties, good flame retardancy and high thermal stability. Thus, we provide a new approach for comprehensive improvement of the properties of these bio-based semi-aromatic polyamide nanocomposite materials.

Received 2nd April 2014
Accepted 1st May 2014

DOI: 10.1039/c4ra02949f

www.rsc.org/advances

1. Introduction

In anticipation of the growing need for sustainable materials for the next century, utilization of natural renewable resources becomes an important consideration.¹ Various materials from nontoxic plant/crop-based resources and biobased renewable products are strategic options that may be considered as alternatives to petroleum-based products. The most widely used renewable resource materials include polysaccharides, vegetable oils, wood and proteins. Various materials have been prepared from these naturally occurring renewable resources.^{2–5} Cyclodextrins belong to the family of cyclic homologous oligosaccharides that are obtained from the enzymatic degradation of starch. Cyclodextrins are composed of six or more α -D-glucopyranose units that are joined at the 1,4 positions by α -glucosidic linkages.⁶ The most commonly used natural

cyclodextrin subtype is β -cyclodextrin, which consists of seven glucose units.

Bio-composites provide an option for the use of new, high performance, “green” composite materials instead of conventional petroleum-based plastic materials. In the preparation of bio-composites and/or polymer nanocomposites, organically modified montmorillonites (O-MMT) are most widely used.^{7–10} Clays are generally organomodified or functionalized in order to form strong interactions between the polymer matrix and nanoclays. Organomodification of clay-Na⁺ is very important for the nanocomposites, since interactions between the polymer matrix and the nanoclays significantly influence the comprehensive properties of polymer nanocomposites. Fornes *et al.*¹¹ investigated the properties of polyamide-6 (PA6)/montmorillonite by using different organic modifiers, and found that the surfactant structure affected the morphology and properties of nylon 6 nanocomposites. It is found that most conventional modifiers of clay are flammable, and that the flammability of these materials ultimately limits the flame retardant properties of polymer nanocomposites. Therefore, modifiers with low flammability and strong interactive properties become very important in the development of high performance clay based polymer nanocomposites. As an example of this, Wang *et al.* have developed a β -cyclodextrin-based layered double hydroxide (LDH) material with low flammability.¹²

Aromatic polyamides (a group of versatile high-performance polymers) display a wide range of applications and properties,

^aMadrid Institute for Advanced Studies of Materials (IMDEA Materials), C/Eric Kandel, 2, 28906 Getafe, Madrid, Spain. E-mail: deyi.wang@imdea.org

^bLeibniz-Institut für Polymerforschung Dresden e.V., Hohe Strasse 6, D-01069 Dresden, Germany

^cFaculty of Chemistry and Petrochemical Engineering, Standard Research Institute (SRI), P.O. Box 31745-139, Karaj, Iran

^dTechnische Universität Dresden, Institut für Werkstoffwissenschaft, D-01069 Dresden, Germany

† Electronic supplementary information (ESI) available. See DOI: 10.1039/c4ra02949f

and are useful for advanced technologies.^{13,14} However, their low solubility and high glass transition temperature often provide problems with their application. In order to address these problems, the use of semi-aromatic polyamides (synthesized *via* a combination of aliphatic and aromatic monomers) is regarded as a promising alternative. Semi-aromatic polyamides are generally exploited to fill the “performance gap” between high-performance polymers and nylons such as PA6.¹⁵ Such polyamides offer a wide range of properties including transparency, outstanding strength-to-weight ratios, high thermal resistance, and good barrier and solvent resistant properties, respectively.^{16–21} In our latest work, a novel biobased semi-aromatic polyamide (BPA) derived from nonanedioic acid and aromatic diamine containing a pyridine group has been synthesized and characterized.²² However, it has been found that while the use of conventional nanoclay (Cloisite 30B) can slightly improve the flame retardancy of BPA materials, it also severely decreases their mechanical properties.

In order to obtain high performance biobased semi-aromatic polyamide (BPA) nanocomposites, two new nanoclays were synthesized and characterized by using two functional modifiers containing modified phosphine oxide and modified β -cyclodextrin, respectively. BPA/organoclay nanocomposites then were prepared *via* solution blending. Effects of the two new organoclays on the morphology, thermal, flammability and mechanical properties of the BPA nanocomposites were investigated, and our findings are reported below.

2. Experimental

2.1 Materials

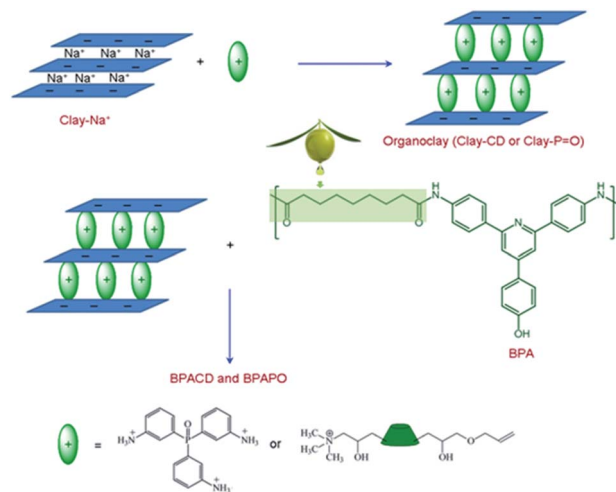
β -cyclodextrin, allyl glycidyl ether (AGE) and (3-chloro-2-hydroxypropyl)trimethylammonium chloride (CMA) were obtained from ABCR GmbH & Co. KG in Germany, and used without further purification. Triphenylphosphine oxide, palladium charcoal, *N*-methyl-2-pyrrolidone (NMP), *N,N*-dimethylacetamide (DMAc), hydrazine hydrate, pyridine, nitric acid, sulfuric acid, methanol, triphenyl phosphite (TPP), oleic acid, 4-nitroacetophenone, 4-hydroxybenzaldehyde, ammonium acetate, potassium permanganate (KMnO₄) and glacial acetic acid obtained from Aldrich were used without further purification. Sodium montmorillonite (NaMMT; unmodified having CEC = 92.6 meq. per 100 g clay) from Southern Clay Products, Inc. was used.

Commercially available calcium chloride (CaCl₂, Aldrich) was dried under vacuum at 150 °C for 6 hours.

2.2 Synthesis of semi-aromatic biobased polyamide (BPA)²²

2.2.1 Synthesis of nonanedioic acid from oleic acid. KMnO₄ was used to oxidize the double bond of the oleic acid, forming nonanedioic acid, following procedures in the literature²³ (yield: 67%).

2.2.2 Synthesis of 4-(4-hydroxyphenyl)-2,6-bis(4-nitrophenyl)pyridine. In a 500 mL round-bottomed flask, a mixture of 5.0 g (41 mmol) of 4-hydroxybenzaldehyde; 13.5 g (82 mmol) of 4-nitroacetophenone; 76.5 g (1.0 mol) of ammonium acetate; and



Scheme 1 Preparation of BPACD and BPAPO.

150 mL of glacial acetic acid were refluxed for 18 hours. Upon cooling, the precipitated yellow solid was collected by filtration and washed with ethanol. The yield of the crude product was 68%, with a melting point of 285 °C (see Scheme 1).

2.2.3 Synthesis of 4-(4-hydroxyphenyl)-2,6-bis(4-aminophenyl)pyridine. In a 250 mL round-bottomed flask equipped with a reflux condenser and a dropping funnel, a suspension of the synthesized dinitro compound (5 g, 12 mmol); palladium on carbon 10% (0.1 g); ethanol (30 mL); and dimethylformamide (DMF, 5 mL) was prepared. The mixture was warmed, and while being stirred magnetically, hydrazine monohydrate 80% (10 mL) in ethanol (15 mL) was added dropwise over a 1 hour period through a dropping funnel, while keeping the temperature at about 70 °C. After 4 hours, the mixture was filtered while hot to remove Pd/C, and the solvent then evaporated under vacuum to afford the yellow solid product (yield, 94%; melting point, 230 °C; ¹H NMR (500 MHz, DMSO) δ , ppm: 9.7 (s, 1H), 8.0 (d, 4H), 7.8 (d, 2H), 7.7 (s, 2H), 6.9 (d, 2H), 6.7 (d, 4H), 5.4 (d, 4H); see Scheme 1).

2.2.4 Synthesis of biobased aliphatic–aromatic polyamide. 4-(4-hydroxyphenyl)-2,6-bis(4-aminophenyl)pyridine (5 g, 14 mmol); nonanedioic acid (2.7 g, 14 mmol); calcium chloride (0.5 g, 4.5 mmol); triphenyl phosphite (8.7 mL, 28 mmol); pyridine (1 mL); and *N*-methyl-2-pyrrolidone (8 mL) were added to a 50 mL round-bottomed flask fitted with a stirring bar. The reaction mixture was heated under reflux in an oil bath at 60 °C for 1 hour, then at 90 °C for 3 hours, and finally at 120 °C for 8 hours. The reaction mixture was then poured into 100 mL of methanol, and the precipitated product collected by filtration and washed thoroughly with hot methanol. Finally, the product was dried at 60 °C for 12 hours in a vacuum oven until a constant weight was attained (yield, 95%).

2.3 Synthesis of β -cyclodextrin based modifier (CD-DB-N+) and tris(3-aminophenyl)phenyl phosphine oxide based modifier

In a 50 mL round-bottomed flask, 4.54 g β -CD (4 mmol) was added with stirring to an aqueous solution composed of 15 mL

water and 3.0 g NaOH maintained at 70 °C. Subsequently, 1.83 g (16 mmol) AGE was slowly added, and the mixture was stirred for 6 hours. Following this, 5.45 g (40 mmol) CMA solution was slowly added with vigorous stirring. After the reaction was complete, the solution was cooled to room temperature and diluted with 30 mL water. The resulting solution was neutralized with 1 M hydrochloric acid and dialyzed against 3 × 700 mL water to remove salts (3-allyloxy-1,2-propanediol and hydroxyalkyl ammonium, respectively) formed as side products. The dialysate was then poured out into 100 mL of ethanol. The precipitate was filtered and dried under vacuum at 80 °C for 12 hours.

Triamine containing phosphorus was synthesized in the laboratory according to the procedure reported elsewhere.²⁴

2.4 Functional modification of nanoclays

Clay-CD was prepared by a cation exchange method. Clay-Na (5 g) was dispersed in 700 mL distilled water at room temperature. Another solution containing 2 g of CD-DB-N⁺ in 40 mL distilled water was prepared using magnetic stirring, and with the addition of 1.0 M HCl aqueous solution to adjust the pH value to 3–4. This solution was added to the clay suspension at a rate of approximately 15 mL min⁻¹ with vigorous stirring. The mixture was stirred overnight at room temperature. Afterward, the organoclay was filtering using a Buchner funnel. The resulting organoclay (clay-CD) was washed with distilled water to remove any excess ammonium ions. The same procedure was used to prepare the organoclay based on the cationic form of TAP (clay-P=O).

2.5 Preparation of BPA/organoclay nanocomposites

The nanocomposites were synthesized by taking the BPA solution in a flask, followed by the addition of an appropriate amount of the organoclay at particular concentrations (see Scheme 1). For example, to prepare a nanocomposite containing 2 wt% of clay-CD, 0.98 g of the BPA was dissolved in DMAc in a 50 mL flask, followed by the addition of 0.02 g of clay-CD. The reaction mixture was agitated at high speed at 25 °C overnight to disperse clay platelets uniformly in the BPA matrix. The amount of clay-CD was 2 and 4 wt% in the nanocomposites (BPACD 2 and BPACD 4), respectively. By casting the suspension onto a glass plate followed by solvent evaporation in a vacuum oven, the final BPA nanocomposite films were prepared. The nanocomposites with the BPA and clay-P=O (BPAPO 2 and BPAPO 4) were prepared using the same procedure.

2.6 Characterization

¹H-NMR measurements were performed with a Bruker Avance III 500 spectrometer (Rheinstetten, Germany) operating at 500 MHz. DMSO-d₆ was used as the solvent and the solvent signal was used for internal calibration (DMSO-d₆: δ(¹H) = 2.5 ppm).

Morphological analysis was carried out using a LEO 912 transmission electron microscope. The conditions used during analysis were room temperature, 120 kV acceleration voltage, and bright field illumination.

Wide angle X-ray scattering (WAXS) was performed using a 2-circle diffractometer XRD 3003 θ/θ (GE Inspection Technologies/Seifert-FPM, Freiberg, Germany) with Cu-K_α radiation (λ = 0.154 nm) generated at 30 mA and 40 kV in the range of 2θ = 2–12° using 0.05° as the step length.

Thermal stability of the samples was investigated by thermogravimetric analysis (TGA; TA instruments Q 5000) in the range between room temperature and 800 °C at a heating rate of 10 °C min⁻¹ in a nitrogen atmosphere. The glass transition temperatures of samples were measured by differential scanning calorimetry (DSC, TA instrument Q1000) in the range between 80 °C and 230 °C at a heating rate of 10 °C min⁻¹ in a nitrogen atmosphere.

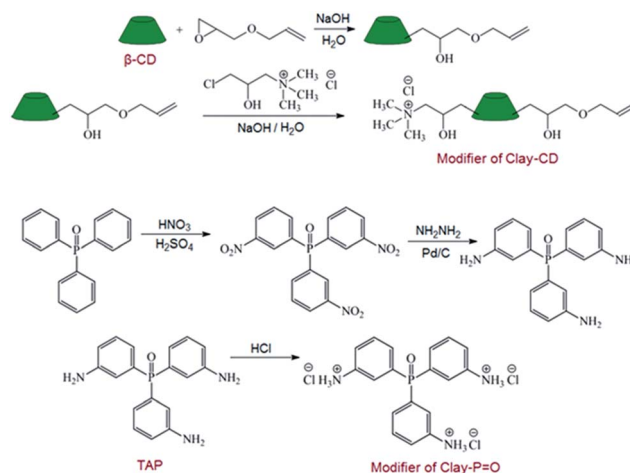
Microscale combustion calorimetry (MCC-1, FTT) is a convenient and relatively new technique developed in recent years for investigating the flammability of polymers.^{25,26} Using this technique, samples of approximately 5 mg mass were heated to 700 °C at a heating rate of 1 °C s⁻¹ in a stream of nitrogen flowing at 80 cm³ min⁻¹. The volatile, anaerobic thermal degradation products were then mixed with a 20 cm³ min⁻¹ gas stream containing 20% oxygen and 80% nitrogen, respectively, prior to entering a 900 °C combustion furnace.

Tensile testing of the films was performed with FAVIGRAPH semiautomatic instrumentation (Textechno Company, Germany), equipped with a 100 N load cell. Specimens of 20 mm gauge length, 40–60 μm thickness, and 3 mm width were tested at a speed of 10 mm min⁻¹. Relative humidity was kept at 50% and the temperature at 23 °C. Modulus strain between 0.1–0.2% was determined by stress–strain curve analysis.

3. Results and discussion

3.1 Synthesis and characterization of functional modifiers

The modified β-cyclodextrin was obtained by the reaction of hydroxyl groups in β-cyclodextrin with the electrophilic groups of AGE and CMA *via* a two-step reaction (Scheme 2). Structure conformation was determined by means of ¹H NMR. As shown in Fig. 1, the singlet peak at 5.87 ppm was assigned to the



Scheme 2 The structure and synthesis route of the two modifiers.

proton on the carbon carbon double bonds ($-\text{CH}=\text{CH}_2$) on the structure of AGE segments (corresponding to C_1 in Fig. 1), while the peak at 4.21 ppm was assigned to protons on the CMA segment (corresponding to C_3 in Fig. 1). All these NMR characteristic peaks matched the expected CD-DB- N^+ structure. During the reaction, the protons of C_2 on β -CD (Fig. 2) were not affected. For this reason, the ratio of the integrated peak for C_2 -H over that of C_1 -H at 5.87 ppm and C_4 -H at 3.25 ppm was used to estimate the number of carbon carbon double bonds and cationic segments grafted. By calculation, the ratio of C_4 -H/ C_2 -H was 7.28, indicating that 5.66 cationic segments were attached per β -CD molecule. The ratio of C_1 -H/ C_2 -H was 0.75, indicating that 5.25 carbon carbon double bonds were attached per β -CD molecule.

TAP was synthesized from triphenyl phosphine oxide, and first converted to tris(3-nitrophenyl)phenyl phosphine oxide by using concentrated nitric acid in the presence of sulfuric acid. Tris(3-nitrophenyl)phenyl phosphine oxide was then reduced to TAP with Pd/C and NH_2NH_2 (Scheme 1).

^1H NMR (500 MHz, DMSO) δ , ppm of TAP: 7.10–7.14 (m, 3H), 6.84–6.87 (d, 3H), 6.71–6.73 (d, 3H), 6.62–6.65 (q, 4H), 5.33 (s, 6H).

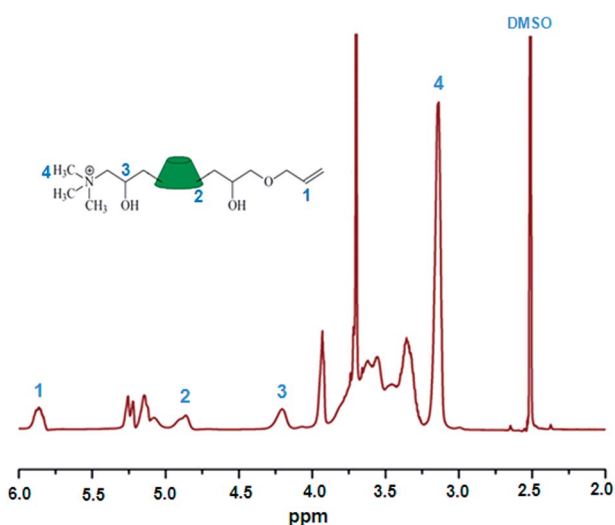


Fig. 1 ^1H NMR spectra of CD-DB- N^+ .

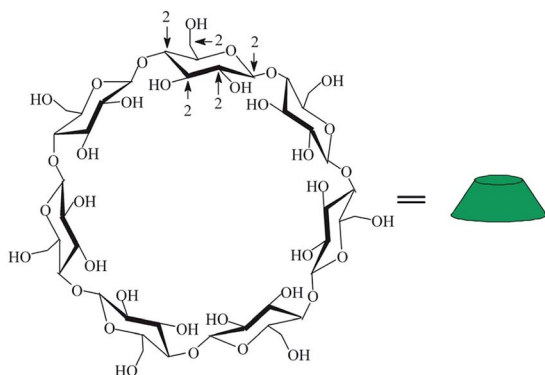


Fig. 2 The structure of β -cyclodextrin (β -CD).

3.2 Characterization of the nanocomposites

3.2.1 X-ray diffraction. XRD patterns of each organoclay and its corresponding nanocomposite are shown in Fig. 3. XRD provided information on the change of interlayer spacing of the clay upon formation of a nanocomposite. X-ray results of modified nanoclays revealed that intercalation behaviors were successfully accomplished by using the new modifiers of CD-DB- N^+ and TAP- N^+ . More specifically, the interlayer d -spacing of the nanoclays increased after the ion-exchange process by the modifiers in comparison to that of the clay- Na^+ . For example, the d -spacing of unmodified clay (clay- Na^+) is 1.17 nm, calculated from the reflection at $2\theta = 7.6^\circ$ using Bragg's equation. After the ion-exchange reaction with the ammonium salt of TAP, reflection of the clay shifted to a new position at $2\theta = 5.4^\circ$ ($d = 1.63$ nm) in clay-P=O. An increase of the interlayer distance led to a shift of the reflection and an increase in the basal spacing, providing evidence that intercalation had occurred. Similarly, it was noted that the d -spacing of clay-CD was 1.42 nm which was calculated from the reflection at $2\theta = 6.2^\circ$. These findings indicate that the functional nanoclays, clay-P=O and clay-CD, were prepared successfully.

Fig. 3 also displays XRD patterns of BPA and corresponding nanocomposites. Composite films containing 2 and 4 wt%, respectively, of the two different organoclays showed no peak in the region $2\theta = 2$ –12. No peaks in XRD patterns were observed for the BPA nanocomposites. This might mean that the organoclays dispersed homogeneously in the form of individual layers within the polymer matrix, or might be suggestive of the preferred orientation effect. Therefore, the absence of a diffraction peak could not be taken as proof for the formation of an exfoliated nanocomposite, and additional evidence based on transmission electron microscopy was required.

Thermal stability of the nanoclays was investigated under nitrogen conditions. Thermogravimetric analysis (TGA) and derivative thermogravimetric analysis (DTG) results of clay- Na^+ , clay-CD and clay-P=O are shown in Fig. 4. Compared to the thermal stability of clay- Na^+ , the modified clays (clay-CD,

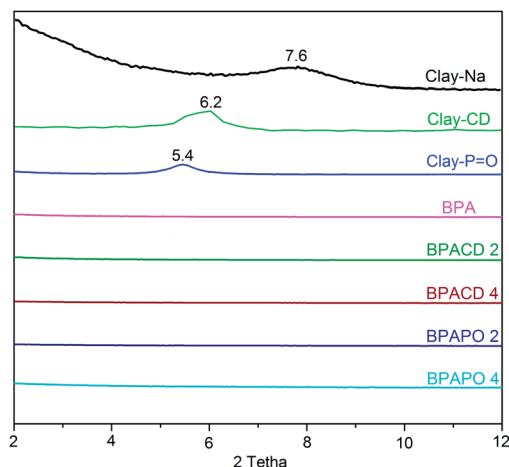


Fig. 3 XRD of the clay- Na^+ , clay-CD, clay-P=O, BPA and different BPA/organoclay nanocomposites.

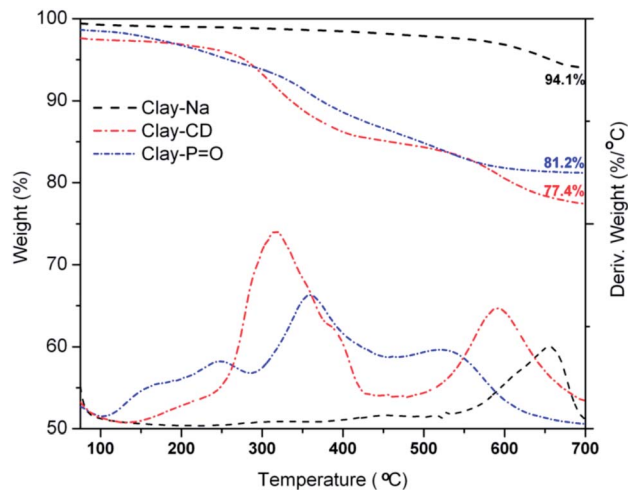


Fig. 4 TGA and DTG results of the clay- Na^+ , clay-CD, clay-P=O in nitrogen conditions (heating rate: $10\text{ }^\circ\text{C min}^{-1}$).

clay-P=O) showed relatively low initial decomposition temperatures. Additionally, their char residues at $700\text{ }^\circ\text{C}$ were very different. For clay- Na^+ , the weight loss between 450 and $700\text{ }^\circ\text{C}$ corresponded to the condensation of silanol groups in the clay; however, for the modified clays, the weight loss between these temperatures was caused by the thermal degradation of the intercalated modifiers. As shown in Fig. 4, the char residue of clay- Na^+ was $94.1\text{ wt}\%$, while the char residues of clay-CD and clay-P=O were $77.4\text{ wt}\%$ and $81.2\text{ wt}\%$, respectively. Therefore, if char formation of the organomodifiers at $700\text{ }^\circ\text{C}$ is ignored, the amount of organomodifiers in clay-CD and clay-P=O are $16.7\text{ wt}\%$ and $12.9\text{ wt}\%$, respectively.

3.2.2 Morphology of the nanocomposites. Transmission electron microscopy presented an actual image of clay platelets to permit identification of the internal morphology of the nanocomposites. This served as a complement to XRD, especially when peaks were not observed in the diffraction patterns. To observe the morphological structure of the bio-based PA nanocomposites, TEM (at both low and high magnification for the composition containing $2.0\text{ wt}\%$ of the organoclays) was carried out. In Fig. 5, a display of BPA nanocomposites based on both the organoclays shows a non-homogeneous distribution in some orientations. Aggregation of the organoclay also was observed. In the case of BPACD 2, some exfoliated nanolayers were found in the polymer matrix, and its agglomeration behaviors were slightly better than those of BPAPO 2. Since BPA nanocomposites did not form full exfoliated structures in either BPACD or BPAPO, how do we explain the fact that no reflection peaks of BPA nanocomposites are indicated in the XRD measurements? The reason for this might correspond to the thickness of the BPA nanocomposite specimens. We noticed that the thickness of each BPA nanocomposite specimen used in this study was only around $50\text{ }\mu\text{m}$, which might be too thin to form an effective reflection.

3.2.3 Thermal properties of the nanocomposites. Thermal stability is a very important factor for polymeric materials, and normally this is indicated by thermogravimetric analysis (TGA)

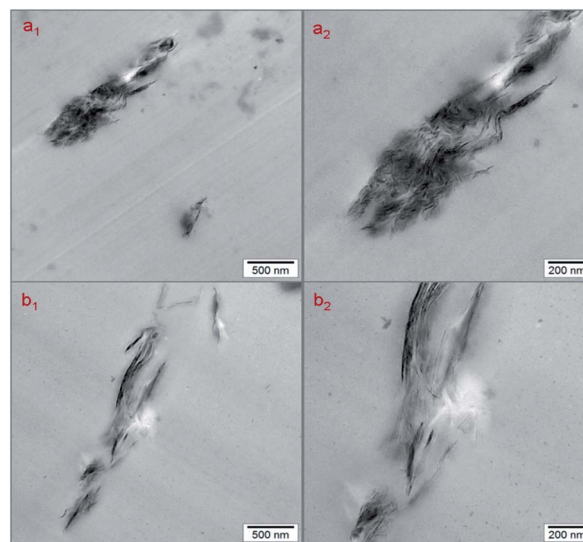


Fig. 5 Low magnification and high magnification TEM images of the nanocomposites: (a) BPAPO 2 and (b) BPACD 2.

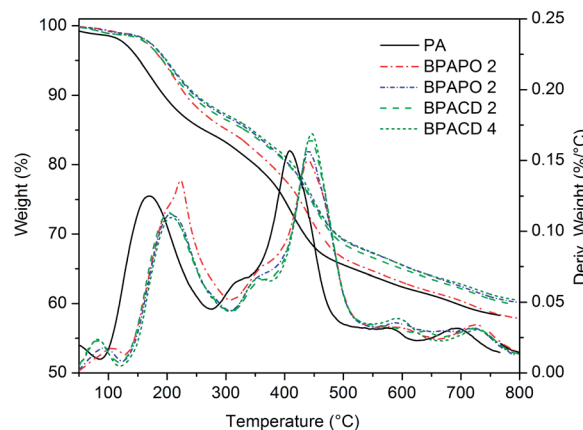


Fig. 6 TGA and DTG curves of BPA and the nanocomposites.

and derivative thermogravimetric analysis (DTG). Fig. 6 shows TGA and DTG curves of the samples, and corresponding data are illustrated in Table 1. The neat BPA showed initial weight loss below $200\text{ }^\circ\text{C}$ due to the removal of moisture and some small organic compounds. The DTG curve indicated that the neat BPA exhibited two decomposition steps with maximum decomposition temperatures at $168\text{ }^\circ\text{C}$ and $409\text{ }^\circ\text{C}$, respectively. After adding clay-P=O and clay-CD, the nanocomposites were more stable than BPA, showing significant increases at the $5\text{ wt}\%$ weight loss temperature (T_5) and the $10\text{ wt}\%$ weight loss temperature (T_{10}). T_5 and T_{10} of all the nanocomposites were higher than those of the neat BPA. Considering the TGA and DTG curves of nanocomposites, we find that the organoclays had a significant effect on the thermal degradation process of BPA. The thermal stability of the nanocomposites increased due to the higher barrier/shielding effect resulting from the clay content in the matrix polymer. Both of the organoclays displayed excellent barrier effects to prevent thermal degradation

Table 1 Thermal property data of the samples

Samples	T_{initial}^a (°C)	T_{10}^b (°C)	$T_{\text{max}1}^c$ (°C)	$T_{\text{max}2}$ (°C)	Char ^d yield	T_g^e
BPA	153	195	168	409	58.3	130
BPACD 2	188	236	205	444	59.8	165
BPACD 4	195	246	205	447	60.5	138
BPAP0 2	192	233	223	439	58.1	133
BPAP0 4	194	243	205	439	60.2	148

^a Temperature at which 5% weight loss was recorded by TGA at a heating rate of $10\text{ }^\circ\text{C min}^{-1}$. ^b Temperature at which 10% weight loss was recorded by TGA at a heating rate of $10\text{ }^\circ\text{C min}^{-1}$. ^c Maximum decomposition temperatures. ^d Weight percentage of material left after TGA analysis at a maximum temperature of $800\text{ }^\circ\text{C}$. ^e Glass transition temperature recorded at a heating rate of $10\text{ }^\circ\text{C min}^{-1}$ in a nitrogen atmosphere.

of polymer chains at relatively low temperatures. The clay layers present in the BPA matrix restricted the diffusion of heat to its bulk, and thus delayed the degradation process. Upon inspection of the char residues of the samples at $800\text{ }^\circ\text{C}$, we note that overall, the nanocomposites slightly improved the char residue at high temperature.

The glass transition temperature (T_g) of the neat BPA and the nanocomposites were investigated using differential scanning calorimetry (DSC), and the results are given in Table 1. The first heating run of DSC was ignored due to the influence of thermal annealing history, and thermal properties were evaluated according to the DSC curves of the second heating (Fig. 7). It was found that addition of the nanoclays caused an increase in the T_g . This suggests that movement of the BPA chains is restricted by the layers of organoclay, thereby increasing the T_g values of the nanocomposites. Among the two types of organoclay with different loading, BPACD 2 gave the greatest increase in T_g value ($T_g = 165\text{ }^\circ\text{C}$) compared to neat BPA. The order of the T_g of the nanocomposites was BPACD 2 > BPAP0 4 > BPACD 4 > BPAP0 2 > BPA.

3.2.4 Flammability of polymer nanocomposites investigated by MCC. Microscale combustion calorimetry (MCC) was used to study the flammability of BPA and the nanocomposites (Fig. 8). The parameters measured from MCC were heat release rate (HRR) (calculated from oxygen depletion measurements),

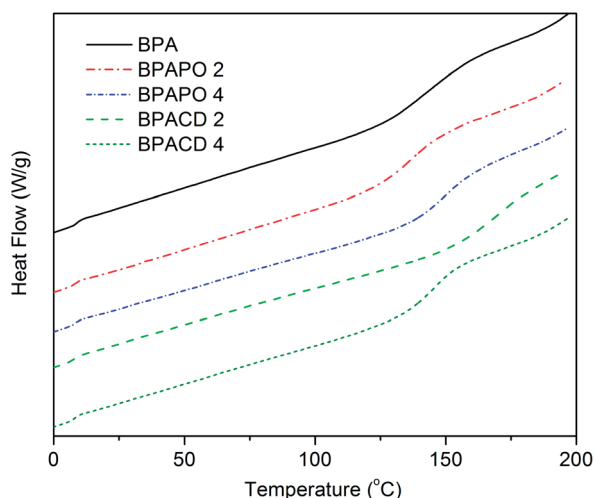


Fig. 7 DSC curves of BPA and the nanocomposites.

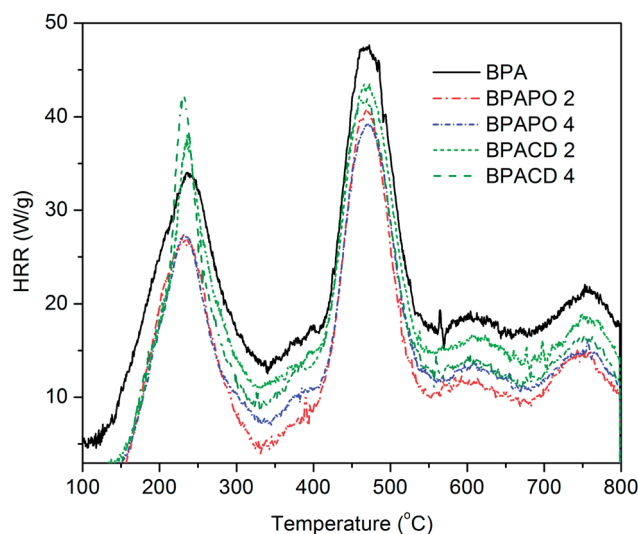


Fig. 8 Flammability of BPA and its nanocomposites by MCC.

and the total heat release (THR) (given by integration of the HRR curve). From Table 2, it may be seen that neat BPA had a peak HRR value (pHRR) of 47.6 W g^{-1} and a THR value of 14.7 kJ g^{-1} . In comparison, by introducing 2 wt% of clay-CD, the pHRR and THR values of BPACD 2 decreased greatly. When the loading of clay-CD was increased to 4 wt%, the pHRR and THR values of BPACD 4 were further reduced to 42.1 W g^{-1} and 11.4 kJ g^{-1} , respectively. For the nanocomposites based on clay-P=O, both BPAP0 2 and BPAP0 4 exhibited even lower pHRR and THR values, indicating that the improvement of flame retardancy in this system was not completely due to the char yield (see Table 2). The decreased pHRR and THR with a small amount of clay-P=O was attributed to compounds with low volatility released during the degradation procedure. The best pHRR and THR values were obtained by adding 4 wt% clay-P=O (pHRR = 38.9 W g^{-1} and THR = 8.6 kJ g^{-1}). In addition to the impact of

Table 2 Data recorded in MCC measurements

Samples	BPA	BPACD 2	BPACD 4	BPAP0 2	BPAP0 4
pHRR (W g^{-1})	47.6	43.3	42.1	40.2	38.9
THR (kJ g^{-1})	14.7	12.4	11.4	9.4	8.6

Table 3 Mechanical properties of BPA and its nanocomposites

Samples	Modulus [GPa] (ϵ 0.1–0.2%)	Maximum stress σ_m [MPa]	Strain at σ_m ϵ_m [%]	Tensile strength at break σ_b [MPa]	Strain at σ_b ϵ_b [%]	Work to fracture W [MJ m ⁻³]
BPA	2.2 ± 0.1	59.4 ± 6.5	3.6 ± 0.5	54.6 ± 5.5	4.0 ± 0.8	1.5 ± 0.4
BPACD 2	2.1 ± 0.1	58.2 ± 6.2	3.7 ± 0.5	58.0 ± 6.0	3.7 ± 0.6	1.3 ± 0.4
BPACD 4	2.6 ± 0.1	61.4 ± 4.1	3.2 ± 0.4	61.3 ± 4.1	3.2 ± 0.4	1.2 ± 0.2
BPAP0 2	2.1 ± 0.1	62.8 ± 3.5	4.1 ± 0.3	62.6 ± 3.5	4.1 ± 0.3	1.5 ± 0.2
BPAP0 4	3.0 ± 0.2	69.5 ± 6.6	3.3 ± 0.4	69.5 ± 6.5	3.3 ± 0.5	1.4 ± 0.3

char residues (condensed phase mechanism) on the flame retardancy of BPACD and BPAP0, another flame retardant mechanism might be possible. The phosphine oxide moieties in the clay-P=O might release some phosphorus-containing radicals which can capture the H[•] and HO[•] in the gas phase, so that the flammability of BPA nanocomposites remains low. This would explain why the flammability of BPAP0 was always lower than that of BPACD.

3.2.5 Mechanical properties. Mechanical property data for neat BPA and the nanocomposites are given in Table 3. The nanocomposites were found to be much stiffer than the neat polymer, and the elastic modulus increased with increasing loading of the organoclays. In the BPACD system, the elastic modulus was higher than that of the neat PA and the elastic modulus increased with increasing loading of clay-CD. The maximum modulus value was observed with 4 wt% of clay-P=O in the BPA matrix, providing more stiffness to the materials (stiffness being a function of the aspect ratio). Such improvement of the mechanical properties of BPAP0 may be attributed to the extensive interaction (*via* formation of hydrogen bonding) between the triamine TAP modifier in BPAP0 and the BPA chains. The results also indicate significant increase in tensile strength of BPAP0 and BPACD, compared with that of the neat BPA. The incorporation of these functional organoclays into the polymer chains can reinforce the polymer, giving the observed increase in this important property. When using conventional modified nanoclay (Cloisite 30B), mechanical properties of BPA nanocomposites (*e.g.* tensile strength at break) are severely decreased.²² Intimate blending of the two phases, presumably with chemical bonding between them, provides a combination of some of the best properties of the two components.²⁷ The maximum stress at break (ultimate strength) was found to increase initially with increase in clay-P=O content, and at 4 wt% organoclay, showed a maximum value of 69.5 MPa. Relative to the corresponding 59.4 MPa value for neat BPA, this represents significant enhancement.

4. Conclusions

Since design and selection of functional nanoclays are very important for preparing polymer nanocomposites, two novel organoclays containing modified phosphine oxide (TAP) and functional β -CD were synthesized *via* ion-exchange reaction. Two types of BPA nanocomposites, BPACD and BPAP0, were produced by solution blending. TEM results indicated the

formation of a non-homogeneous distribution in some orientations of the nanocomposites. Thermal stability of BPA nanocomposites was improved compared with neat BPA, and in particular, clay-CD based nanocomposites showed more improvements. The improvement in thermal stability of BPA nanocomposites was attributed primarily to the physical barrier effect of the organoclays. Flammability of the BPA nanocomposites with different nanoclay concentrations was investigated by microscale combustion calorimetry (MCC). It was found that clay-P=O had the best effect on improving the flame retardancy of BPA, showing the lowest values of peak heat release rate (pHRR) and total heat release (THR) of the BPA nanocomposites. With the increase of clay-P=O loading, the BPA nanocomposites showed improved flame retardancy. In the case of clay-CD based nanocomposites, mechanical properties and flame retardancy of BPACD also increased with the increase of nanoclay loading. In comparison, clay-P=O based nanocomposites showed even greater improvements in flame retardancy and mechanical properties. Besides the char residue impact on flame retardancy of both BPACD and BPAP0, another possible flame retardant mechanism for BPAP0 involves phosphine oxide moieties in the clay-P=O releasing some phosphorus-containing radicals which can capture the H[•] and HO[•] in the gas phase, so that the flammability of BPA nanocomposites remains low. Here, we have systematically investigated and described the effects of functional organoclays on flammability, thermal and mechanical properties of BPA nanocomposites. Our findings strongly suggest that these sustainable biobased semi-aromatic polyamide/functional clay nanocomposites have great potential for being used to develop high performance materials in different areas.

Acknowledgements

This research is partly funded by the European Commission under the 7th Framework Programme (Marie Curie Career Integration Grant) and Ramón y Cajal grant.

Notes and references

- 1 Y. Parulekar and A. K. Mohanty, *Green Chem.*, 2006, **8**, 206–213.
- 2 C. K. Williams and M. A. Hillmyer, *Polym. Rev.*, 2008, **48**, 1–10.
- 3 Y. Xia and R. C. Larock, *Green Chem.*, 2010, **12**, 1893–1909.

- 4 J. Zuo, S. Li, L. Bouzidi and S. S. Narine, *Polymer*, 2011, **52**, 4503–4516.
- 5 M. Haq, R. Burgueño, A. K. Mohanty and M. Misra, *Composites, Part A*, 2009, **40**, 540–547.
- 6 F. van de Manakker, T. Vermonden, C. F. van Nostrum and W. E. Hennink, *Biomacromolecules*, 2009, **10**, 3157–3175.
- 7 C. A. Diaz, Y. Xia, M. Rubino, R. Auras, K. Jayaraman and J. Hotchkiss, *Nanoscale*, 2013, **5**, 164–168.
- 8 T. Jiang, Y.-h. Wang, J.-t. Yeh and Z.-q. Fan, *Eur. Polym. J.*, 2005, **41**, 459–466.
- 9 D. Y. Wang, U. Gohs, N. J. Kang, A. Leuteritz, R. Boldt, U. Wagenknecht and G. Heinrich, *Langmuir*, 2012, **28**(34), 12601–12608.
- 10 D. Y. Wang, Y. P. Song, J. S. Wang, X. G. Ge, Y. Z. Wang, A. A. Stec and T. R. Hull, *Nanoscale Res. Lett.*, 2009, **4**, 303–306.
- 11 T. D. Fornes, P. J. Yoon, D. L. Hunter, H. Keskkula and D. R. Paul, *Polymer*, 2002, **43**, 5915–5933.
- 12 N. J. Kang and D. Y. Wang, *J. Mater. Chem. A*, 2013, **1**(37), 11376–11383.
- 13 M. Trigo-Lopez, P. Estevez, N. San-Jose, A. Gomez-Valdemoro, F. C. Garcia, F. Serna, J. L. d. l. Pena and J. M. Garcia, *Recent Pat. Mater. Sci.*, 2009, **2**, 190–208.
- 14 M. Shabaniyan and N. Basaki, *Composites, Part B*, 2013, **52**, 224–232.
- 15 S. Zulfiqar, A. Kausar, M. Rizwan and M. I. Sarwar, *Appl. Surf. Sci.*, 2008, **255**, 2080–2086.
- 16 A. S. Patil, M. Medhi, N. V. Sadavarte, P. P. Wadgaonkar and N. N. Maldar, *Mater. Sci. Eng., B*, 2010, **168**, 111–116.
- 17 A. L. Chen, K. L. Wei, R. J. Jeng, J. J. Lin and S. A. Dai, *Macromolecules*, 2010, **44**, 46–59.
- 18 Y. Ito, T. Higashihara and M. Ueda, *Macromolecules*, 2012, **45**, 4175–4183.
- 19 S. Shabbir, S. Zulfiqar, Z. Ahmad and M. I. Sarwar, *Tetrahedron*, 2010, **66**, 7204–7212.
- 20 M. Shabaniyan, N. J. Kang, D. Y. Wang, U. Wagenknecht and G. Heinrich, *Polym. Degrad. Stab.*, 2013, **98**, 1036–1042.
- 21 M. Shabaniyan, N. Kang, D. Y. Wang, U. Wagenknecht and G. Heinrich, *RSC Adv.*, 2013, **3**, 20738–20745.
- 22 M. Shabaniyan, H. Moghanian, J. W. Liu, U. Wagenknecht, G. Heinrich and D. Y. Wang, Novel Aliphatic–Aromatic Polyamide Nanocomposite Derived from Biobased Diacid: Synthesis and Characterization, *Chem. Mater.*, 2013, Submitted.
- 23 J. W. Hill and W. L. McEwen, *Org. Synth.*, 1933, **13**, 4.
- 24 I. K. Varma, G. M. Fohlen and J. A. Parker, *J. Macromol. Sci., Part A: Pure Appl. Chem.*, 1983, **19**, 209–224.
- 25 Y. Shi, T. Kashiwagi, R. N. Walters, J. W. Gilman, R. E. Lyon and D. Y. Sogah, *Polymer*, 2009, **50**, 3478–3487.
- 26 D. Y. Wang, A. Das, F. R. Costa, A. Leuteritz, Y. Z. Wang, U. Wagenknecht and G. Heinrich, *Langmuir*, 2010, **26**, 14162–14169.
- 27 S. Zulfiqar and M. Sarwar, *J. Inclusion Phenom. Macrocyclic Chem.*, 2008, **62**, 353–361.